High-pressure elasticity of calcium oxide: A comparison between Brillouin spectroscopy and radial X-ray diffraction

Sergio Speziale,[1,2] Sean R. Shieh,[3,4] and Thomas S. Duffy[1]

Received 5 May 2005; revised 14 September 2005; accepted 9 November 2005; published 28 February 2006.

[1] Single-crystal Brillouin scattering to 25.2 GPa and powder X-ray diffraction to 65.2 GPa in a radial geometry were carried out on CaO (lime) at ambient temperature in a diamond cell. From Brillouin scattering measurements the isentropic elastic constants of CaO at ambient conditions are C_{11} = 219.4 (7), C_{12} = 58.1 (7), C_{44} = 80.0 (2) GPa, where the numbers in parentheses are 1σ uncertainties on the last digit. The pressure derivatives of the compressional and off-diagonal constants at ambient pressure are $\partial C_{11}/\partial P$ = 9.9 (1), $\partial C_{12}/\partial P$ = 2.2 (1), respectively. The pressure derivative of the shear constant is $\partial C_{44}/\partial P$ = 0.25 (3), and it becomes negative at pressures above 5.9 GPa. Aggregate bulk and shear moduli are K_{S0} = 112.0 (2) and G_0 = 80.05 (9) GPa, and their pressure derivatives are 4.72 (6) and 1.69 (5), respectively. The radial X-ray diffraction data allow us to estimate the yield strength and the elastic constants of CaO using a phenomenological lattice strain model. The calculated strength of CaO increases from 0.3 to 1.9 GPa in the pressure range between 5.6 and 57.8 GPa. The estimated elastic constants are in good agreement with the extrapolation of the Brillouin data up to 36.6 GPa. At higher pressures, C_{11} appears softer and C_{12} appears stiffer than the extrapolation of Brillouin results. The value of C_{44} from radial diffraction is in agreement with the Brillouin data through the entire experimental pressure range. The discrepancies between Brillouin and radial diffraction data for C_{11} and C_{12} can be reconciled if α, the parameter which describes degree of stress/strain continuity across the sample's grains boundary, is allowed to vary from 1 at 36.6 GPa to 0.82 at 65.2 GPa. The "hydrostatic" cell volumes determined by applying lattice strain theory were fitted to the third-order Birch-Murnaghan equation. The fitted bulk modulus and its pressure derivative are K_{T0} = 110 (5) GPa and $(\partial K_T/\partial P)_{T0}$ = 4.5 (4), consistent with the Brillouin results, although possible softening of the equation of state at high pressure has been identified. The general agreement between the results of the two methods indicates that radial diffraction with lattice strain theory is a valid probe of the mechanical properties of a moderately soft cubic solid as CaO at ultrahigh pressures. However, more tests are required to quantify the effect of plasticity and texturing on the results of this method.

Citation: Speziale, S., S. R. Shieh, and T. S. Duffy (2006), High-pressure elasticity of calcium oxide: A comparison between Brillouin spectroscopy and radial X-ray diffraction, *J. Geophys. Res.*, *111*, B02203, doi:10.1029/2005JB003823.

1. Introduction

[2] Elastic properties of minerals at high pressure (and temperature) are required to develop reliable geophysical models of the Earth's deep interior, which integrate cosmochemical and geochemical information with global seismological models [*Duffy and Anderson*, 1989]. The elastic moduli of minerals control the velocity of propagation of seismic waves and knowledge of their pressure, temperature and compositional dependence is necessary to interpret velocity anomalies of seismic tomography models in terms of variations of temperature, composition and mineralogy [*Karato and Karki*, 2001]. Knowing the complete elastic tensor [C_{ij}], instead of just the aggregate bulk and shear moduli, allows us to determine the elastic anisotropy of minerals and helps in interpreting the azimuthal seismic anisotropy in the Earth's interior.

[3] The transition of minerals from elastic behavior to plastic deformation, characterized by their mechanical strength, has a fundamental role in determining the onset of flow in the solid state. Plastic deformation of minerals

[1]Department of Geosciences, Princeton University, Princeton, New Jersey, USA.
[2]Now at Department of Earth and Planetary Science, University of California, Berkeley, California, USA.
[3]Department of Earth Sciences, National Cheng Kung University, Tainan, Taiwan.
[4]Now at Department of Earth Sciences, University of Western Ontario, London, Ontario, Canada.

0148-0227/06/2005JB003823$09.00

is also related to texturing and preferred orientation and produces seismic attenuation phenomena, which generate distinct seismic signatures [*Karato and Wu*, 1993].

[4] The techniques that allow direct measurement of the elastic moduli such as ultrasonic interferometry, resonant ultrasound spectroscopy and Brillouin scattering are presently limited at most to pressures of the uppermost part of the lower mantle [*Zha et al.*, 2000] (also see *Liebermann and Li* [1998] for a review). This limitation has stimulated the development of alternative methods to extract indirect information about the elastic properties at very high pressures.

[5] Radial X-ray diffraction of powder samples compressed in a diamond anvil cell combined with the theory of lattice strain under nonhydrostatic stress [*Singh et al.*, 1998a] allows us to estimate the strength of materials at high pressure. In addition, nonhydrostatic stress conditions produce preferred orientation of aggregates easily detectable by radial X-ray diffraction making this technique suitable for the study of mineral deformation at ultrahigh pressures [*Merkel et al.*, 2002; *Wenk et al.*, 2004].

[6] Understanding the actual stress conditions that are achieved during nonhydrostatic compression of powdered samples in opposed anvil cells and the use of those nonhydrostatic conditions to constrain mechanical properties of materials is a long-standing subject of research, approached both on the theoretical and experimental ground [*Singh and Kennedy*, 1974; *Ruoff*, 1975; *Meade and Jeanloz*, 1988; *Funamori et al.*, 1994; *Matthies et al.*, 2001]. Recently, the difference between the results of X-ray radial diffraction of ε-Fe [*Singh et al.*, 1998b] and high-pressure measurements of sound velocity and elastic constants by inelastic X-ray scattering, Raman scattering, and theoretical computations [*Mao et al.*, 1998; *Steinle-Neumann et al.*, 1999; *Merkel et al.*, 2000; *Antonangeli et al.*, 2004] has raised questions about the reliability of radial X-ray diffraction as a means to constrain the elastic tensor of minerals at pressures. In addition, the incorporation of texturing and of plastic deformation poses serious limitations to the application of the lattice strain theory, which is based on the assumption that the examined material behaves purely elastically [*Matthies et al.*, 2001; *Weidner et al.*, 2004]. In order to further test the reliability of radial X-ray diffraction we have performed a study of CaO in which we compare direct measurements of single-crystal elastic properties by Brillouin scattering with radial X-ray diffraction on the same material subject to nonhydrostatic compression.

[7] CaO is a prototype of binary ionic oxides and the knowledge of its elasticity can improve our basic understanding of metal oxides bonding interactions, which can be used to interpret more complex oxide compounds. CaO is also a chemical component of relevance to the Earth's mantle, and the decomposition of $CaSiO_3$ could allow the presence of CaO as a separate mineral phase in the lower mantle. Finally, CaO undergoes a structural phase transition from NaCl-type structure to CsCl-type at $P = 53-70$ GPa at room temperature [*Jeanloz et al.*, 1979; *Richet et al.*, 1988; *Yamanaka et al.*, 2002]. It has been proposed that the transition is driven by elastic shear instability, caused by vanishing of C_{44} [*Karki and Crain*, 1998]. Probing the elastic behavior of CaO with increasing pressure can allow us to better understand phenomena preceding the elastic destabilization.

2. Samples and Methods

2.1. Brillouin Scattering

[8] A single crystal of CaO obtained from Commercial Crystal Laboratories (Naples, Florida) was cut in a general direction, which was later determined to be (0 0.4 1) and double-side polished to a thickness of 25 μm. CaO is highly hygroscopic, for this reason the single crystal sample was stored in mineral oil and polished and loaded in water-free fluids. The measured lattice constant determined by powder X-ray diffraction is 4.8115 (5) Å, in excellent agreement with the value of 4.8105 Å reported by *Wyckoff* [1963].

[9] Two sets of measurements were performed on two different fragments of the double-side polished plate. In the first experiment Brillouin scattering was measured at 0.75, 2.0, 4.8, 5.9, 7.3, 8.4, 9.7 and 11.1 GPa and then at 17.3 and 23 GPa; in the second experiment measurements were performed at 0.9, 3.2, 5.3, 7.6 and 9.8 GPa and then at 17.9, 18.8 and 25.2 GPa.

[10] In both the experiments, the crystal platelets were loaded in modified Merrill-Bassett diamond anvil cells [*Merrill and Bassett*, 1974] with a 96° aperture angle. Each sample was placed in a cylindrical chamber obtained by drilling a 250-μm diameter hole in a stainless steel gasket preindented to a thickness of 55 μm. The samples were compressed between 500-μm diamond culets. A mixture of methanol and ethanol with volume ratio 4:1 was used as a pressure medium, and a few ruby chips were loaded in the cells as a pressure calibrant [*Mao et al.*, 1986].

[11] We measured pressure both before and after the Brillouin measurements at each loading step. We also waited for 4 hours for stabilization after each pressure increment. In all sets of high-pressure experiments, the R_1 ruby fluorescence line showed broadening with pressure, but until 11.1 GPa the width variation was smaller than 15% of the width at room pressure. The data points collected at higher pressure showed a someway larger broadening of the R_1 peak. The difference between the pressures measured at different positions in the sample chamber never exceeded 0.2 GPa at pressures below 17.3 GPa. The differences increased to 0.4 GPa at the pressures from 17.3 to 25.2 GPa.

[12] Brillouin scattering measurements were carried out using the 532.15 nm line of a Nd:YVO_4 laser. The signal was collected by a Sandercock-type Fabry-Perot multipass tandem interferometer, and measured by a solid-state photon detector with 70% quantum efficiency in the spectral region of interest.

[13] Measurements were performed at room pressure on a thick (2 mm) platelet with the same orientation as the samples loaded in the diamond cell. Both room pressure and high-pressure Brillouin measurements were performed in symmetric forward scattering geometry. The angle between the incident and scattered beam was 110 degree. The exposure time for each spectrum was on average 15 min. Precision and accuracy of the acoustic velocity determinations were tested on standard oxides and are better then 0.5% (at 1σ level). Acoustic velocity was measured in 20 to

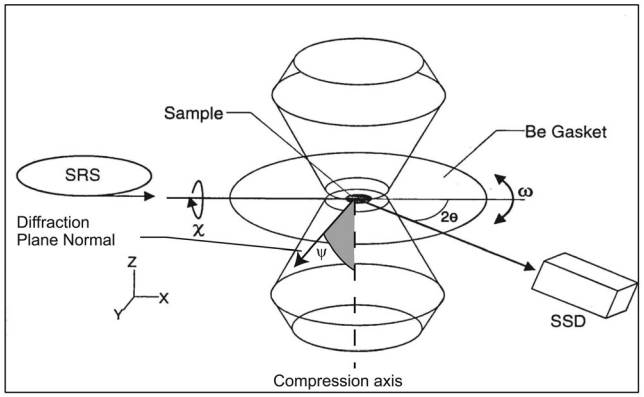

Figure 1. Experimental geometry for radial X-ray diffraction measurements. SRS, NSLS synchrotron light source; ψ, angle between the diffracting plane normal and the compression axis of the diamond cell; 2θ, diffraction angle; χ, ω, rotation angles on the two goniometers of the two circle diffractometer installed at the beam line X17C of NSLS; SSD, solid-state detector.

36 directions at each pressure. Two acoustic modes, one quasi-longitudinal and one quasi-shear were detected.

[14] Particular care was devoted to prevent vignetting effects from the body of the diamond cell [*Oliver et al.*, 1992; *Sinogeikin and Bass*, 2000]. Adjustable slits were placed both along the incident and the scattered light paths and their opening sizes were calibrated performing test measurements on standard materials. A detailed description of the experimental setup is given by *Speziale and Duffy* [2002].

2.2. Radial X-Ray Diffraction Measurements

[15] CaO powder (Alfa Aesar) was ground and homogenized for more than 1 hour to an average 5 μm grain size and loaded in a 70-μm sample chamber drilled in a Be gasket preindented to a pressure of 23 GPa. The powders were gently precompacted and loaded in compact piston-cylinder high-pressure cells. The samples were compressed between 300-μm diamond culets. A single fragment of Mo foil, 5 to 10 μm in diameter, was loaded with each sample. The Mo fragment was placed exactly at the center of the diamond culets as a positioning reference point and as a pressure marker. We selected Mo to prevent overlaps with the diffraction lines of the sample.

[16] Room pressure X-ray diffraction of the CaO powder samples yielded a_0 = 4.8108 (3) Å, in very good agreement with the value determined for the single crystal sample. Because of the high sensitivity of CaO to water, the powder sample was stored in a dry atmosphere and used in the first few hours after the bottle was opened. We tested by X-ray diffraction that in the first 5 hours after the sample was opened no trace of $Ca(OH)_2$ was detectable.

[17] Radial X-ray diffraction experiments were performed in energy dispersive geometry at the X17C beam line of the National Synchrotron Light Source (NSLS) at Brookhaven National Laboratory (Upton, New York). Incident X rays were collimated with slits to 50 μm × 60 μm and then focused to the sample with Kirkpatrick-Baez mirrors to a final 8 μm × 15 μm size. The size of the beam was measured by a sharp opaque edge. The diffracted X rays were collected with a brass collimator with 40 μm aperture, which also operated as a spatial filter. The beam finally passed through a slit system positioned in front of a Ge solid-state detector.

[18] In this set of experiments the incident beam passed "radially" through the Be gasket. The X-ray diffraction was performed using a double circle horizontal diffractometer. The scattering angle 2θ was fixed to 10.000 (1) degrees. The diamond cell was mounted on a vertical goniometer whose rotation axis corresponded to the bisector of the scattering angle. A schematic diagram of the radial X-ray diffraction experimental setup and scattering geometry is given in Figure 1. The X ray was directed to the region of the sample in contact with the Mo marker, in order to collect spectra from the axial region of the sample chamber and to have direct information of the actual experimental pressure using the equation of state of Mo by *Zhao et al.* [2001].

[19] After each pressurization step, spectra were collected at intervals of 15 min until the peaks' positions converged to stable values, indicating a complete stress relaxation of the sample. The relaxation was complete, on average, in 2 h. At the end of the data set collection at a given loading (which lasted on average 6 h) another measurement was performed in the same geometry as that at the beginning. No further relaxation was observed at any pressure.

[20] At each compression step, spectra were collected at 7 values of the angle ψ between the diamonds axis and the diffracting plane normal (ψ = 0°, 24°, 35°, 45°, 55°, 66°, 90°). A more detailed description of the experimental technique is given by *Duffy et al.* [1999a, 1999b].

3. Data Analysis

3.1. Brillouin Scattering

[21] The acoustic velocity was determined from the measured Brillouin frequency shift in forward symmetric geometry [*Withfield et al.*, 1976]:

$$v = \frac{\Delta\nu\lambda_0}{2\sin\alpha}, \tag{1}$$

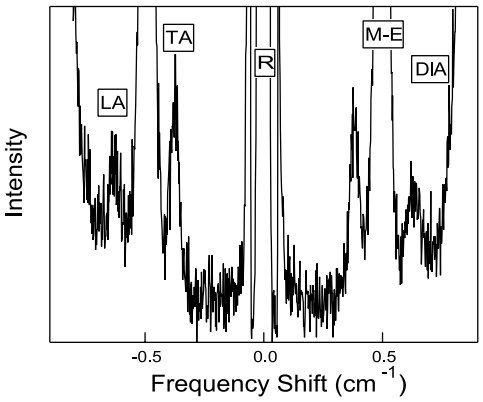

Figure 2. Brillouin spectrum of CaO collected at 8.4 GPa. R, elastic scattering (Rayleigh) peak; LA, quasi-longitudinal acoustic mode; TA, quasi-transverse acoustic mode; DIA, diamond quasi-transverse mode; M-E, methanol-ethanol mixture (4:1 vol. ratio) used as a pressure-transmitting medium.

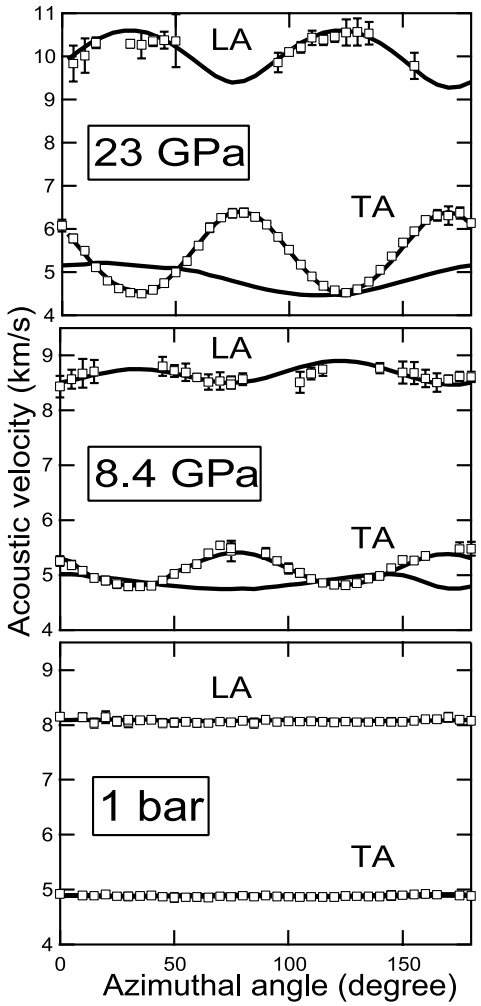

Figure 3. Velocity of the quasi-longitudinal and quasi-transverse acoustic modes in the (0 0.4 1) plane of CaO at 1 bar, 8.4 GPa, and 23 GPa. The azimuthal angle is relative to an arbitrary starting direction. The curves are model velocities calculated using the best fit elastic constants. Abbreviations are as in Figure 2.

where λ_0 is the incident laser wavelength, and α is the external incidence angle. An example spectrum collected at 8.4 GPa is given in Figure 2. CaO crystallizes in the cubic system and it has three nonzero, independent elastic constants: C_{11}, C_{12}, and C_{44}. The elastic constants and the crystal platelet orientation were determined by inversion of the set of velocities measured at each pressure using Christoffel's equation [*Auld*, 1973]

$$\left(C_{iklm}l_k l_m - \rho v^2 \delta_{il}\right)u_l = 0, \tag{2}$$

where C_{iklm} are the elastic constants (in full notation), l_k and l_m are the direction cosines of the phonon, and u_l is the local displacement vector, ρ is the density of the material, δ_{il} is the Kronecker delta. Three velocity data sets collected at 1 bar, 8.4 GPa, and 23 GPa pressure are plotted in Figure 3 together with the calculated velocity model from the inversion results. The uncertainty on the measured transverse velocities is on average 1% of the measurement, while the uncertainty on the longitudinal velocities is 2%. The main reason of this difference is the low intensity of the Brillouin peaks for the longitudinal acoustic mode, caused by modest elasto-optic coupling (Pockel's tensor) in several directions along the investigated crystal plane of CaO.

[22] Voigt and Reuss bounds to the aggregate bulk modulus, K_S, and shear modulus, G, were calculated from the inverted elastic constants at each pressure. The pressure dependence of both the isentropic constants and aggregate moduli was determined by inversion to Eulerian finite strain equations [*Davies and Dziewonski*, 1975]. The room pressure isentropic moduli and constants and their pressure derivatives were converted to isothermal values by means of thermodynamic identities [*Barsch*, 1967] using parameters reported in Table 1.

3.2. Radial X-Ray Diffraction

[23] The radial X-ray diffraction data collected at each pressure (Figure 4) were analyzed following the model developed by *Singh* [1993] and *Singh et al.* [1998a] and here briefly summarized.

[24] The diamond anvil cell is a uniaxial stress device. We define σ_{33} as the maximum stress along the direction of the diamond anvils axes and σ_{11} the minimum stress along the plane orthogonal to the diamonds' axes. The stress state, σ_{ij}, at the center of the sample chamber is given by

$$\sigma_{ij} = \sigma_P + D_{ij}, \tag{3}$$

where $\sigma_P = (2\sigma_{11} + \sigma_{33})/3$ is the hydrostatic stress component and D_{ij} is the deviatoric stress component. We define the quantity $t = (\sigma_{33} - \sigma_{11})$ as the differential stress, whose upper limit is the yield strength (σ_y), equal to twice the shear strength (τ_y) of the sample material at the pressure σ_P.

[25] The measured lattice strain can be expressed as

$$d_m(hkl) = d_P(hkl)\left[1 + \left(1 - 3\cos^2\psi\right)Q(hkl)\right], \tag{4}$$

where $d_m(hkl)$ is the measured d spacing, ψ is the angle between the diamond axis direction and the diffracting plane normal, $d_P(hkl)$ is the d spacing under a hydrostatic pressure σ_P, and $Q(hkl)$ is given by

$$Q(hkl) = t/3\left\{\alpha[2G_R(hkl)]^{-1} + (1-\alpha)(2G_V)^{-1}\right\}, \tag{5}$$

where $G_R(hkl)$ is the microscopic shear modulus for the isostress condition (Reuss model) and G_V is the shear

Table 1. Thermoelastic Parameters of CaO at Ambient Conditions

Parameter	Value[a]	Reference
Thermal expansivity α	$-3.04\ (2) \times 10^{-5}$ K^{-1}	*Oda et al.* [1992]
Specific heat C_P	-75.2 J kg^{-1} K^{-1}	*Garvin et al.* [1987]
Grüneisen parameter γ	-1.35 (9)	calculated[b]
$(\partial K_S/\partial T)_{P0}$	-0.0143 (1) GPa K^{-1}	*Oda et al.* [1992]
$(\partial K_T/\partial T)_{P0}$	-0.0203 (2) GPa K^{-1}	calculated[c]

[a]Numbers in parentheses are 1 standard deviation uncertainty in the last digits.

[b]Grüneisen parameter obtained as $\gamma = \alpha K_{S0}/(\rho_0 C_P)$, where ρ_0 is density at ambient conditions.

[c]Calculated as $(\partial K_T/\partial T)_{P0} \cong (\partial K_S/\partial T)_{P0}/(1 + \alpha\gamma T) - K_{S0}/(1 + \alpha\gamma T)^2 [\alpha\gamma + (\partial\alpha/\partial T)\gamma T]$, where T is temperature (K).

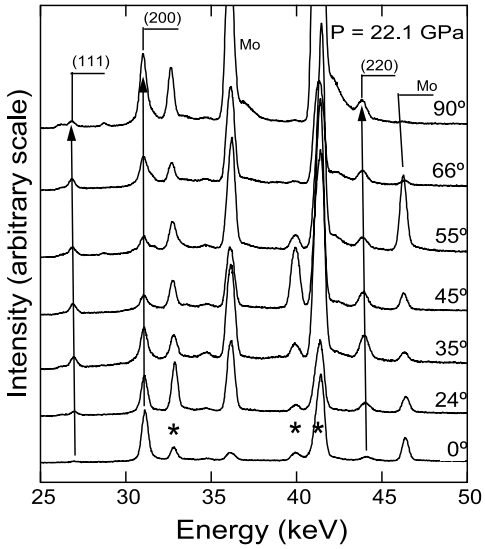

Figure 4. X-ray diffraction patterns collected at a hydrostatic pressure of 22.1 GPa at different values of the angle ψ (angle between the diffracting plane normal and the compression axis of the diamond cell). Mo, molybdenum marker; Be, beryllium gasket. Asterisks indicate diffraction peaks from the beryllium gasket.

modulus for the isostrain condition (Voigt model). They are expressed as

$$[2G_R(hkl)]^{-1} = S_{11} - S_{12} - 3(S_{11} - S_{12} + 0.5S_{44})\Gamma(hkl),$$
$$(2G_V)^{-1} = 5/2(S_{11} - S_{12})S_{44}/[3(S_{11} - S_{12}) + S_{44}], \quad (6)$$

where S_{ij} are the elastic compliances of the sample material at the pressure σ_P, and $\Gamma(hkl) = (h^2k^2 + k^2l^2 + l^2h^2)/(h^2 + k^2 + l^2)^2$ is an orientation-dependent factor.

[26] We fixed the parameter α to the value of 1 corresponding to stress continuity across the grain boundaries in the sample [*Funamori et al.*, 1994]. Weighed linear fitting of the observed d spacings of the three lattice planes families (111), (200), and (220) of CaO to equation (4) allowed us to determine the "hydrostatic" strains $d_P(hkl)$ and the parameter Q(hkl) for the three different examined lattice planes (Figure 5). The diffraction peaks of the two lattice plane families (110) and (200) of the Mo marker were also inverted using equation (4) and the "hydrostatic" pressure, σ_P, in the sample chamber was determined using molybdenum equation of state of *Zhao et al.* [2001].

[27] Fitting of $Q(hkl)$ and the factor $\Gamma(hkl)$ using a linear relation (Figure 6) allowed us to directly determine the Zener anisotropy factor $A = 2(S_{11} - S_{12})/S_{44} = 2C_{44}/(C_{11} - C_{12})$. From the elastic anisotropy, we could estimate the uniaxial stress component $t = \sigma_{33} - \sigma_{11}$, using the relation [*Singh et al.*, 1998b]

$$t = 6G\langle Q(hkl)\rangle F(A, \alpha), \quad (7)$$

where G is the aggregate shear modulus appropriate for the boundary conditions defined by the parameter α, $\langle Q(hkl)\rangle$ is the average of the $Q(hkl)$ values of the lattice plane families, and $F(A, \alpha)$ is a function of the anisotropy factor and of the parameter α [see *Singh et al.*, 1998a, 1998b]. Combining

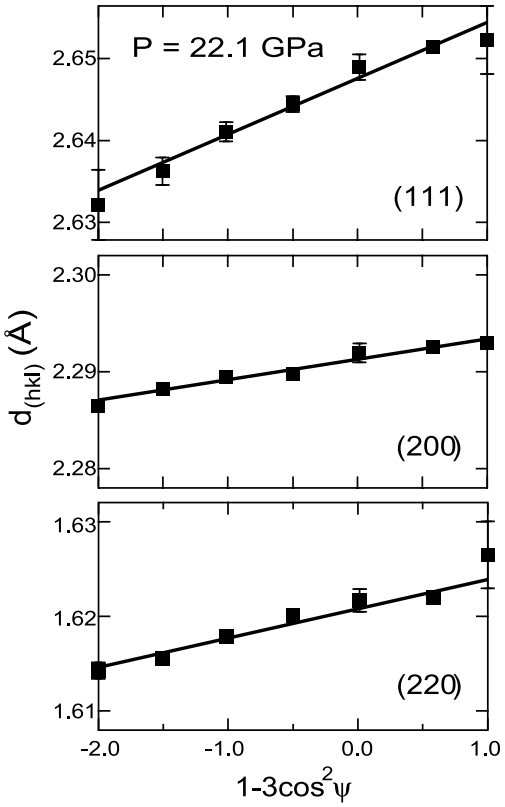

Figure 5. Dependence of the d spacing on $1-3\cos^2\psi$ for the lattice plane families (111), (200), (220) of CaO at a hydrostatic pressure σ_P of 22.1 GPa (see text for explanations).

the parameters t, $Q(hkl)$, A, and $\Gamma(hkl)$, directly obtained from the X-ray radial diffraction data with the high-pressure bulk modulus and the shear modulus extrapolated from single-crystal Brillouin scattering, we could calculate the full elastic compliance tensor at each experimental pressure [e.g., *Singh et al.*, 1998b].

4. Results and Discussion

4.1. Brillouin Scattering

[28] The measured velocities, phonon orientations along the sample plane and a starting density model were itera-

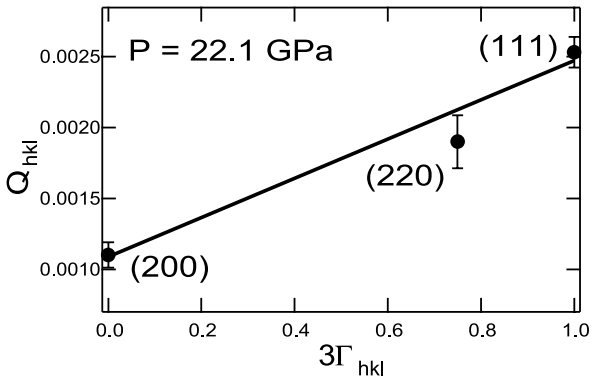

Figure 6. $Q(hkl)$ as a function of $3\Gamma(hkl)$ for CaO at a hydrostatic pressure of 22.1 GPa (see text for explanations).

Table 2. Density and Elastic Constants of CaO by Brillouin Scattering[a]

Pressure, GPa	ρ, Mg m^{-3}	C_{11}, GPa	C_{12}, GPa	C_{44}, GPa	RMS, m s^{-1}	Number of Data
10^{-4}	3.344	219.4 (7)	58.1 (7)	80.0 (2)	28	65
0.75	3.366	224.6 (20)	60.1 (23)	79.4 (5)	26	49
0.9	3.371	225.4 (20)	60.4 (17)	80.2 (9)	45	32
2.0	3.403	242.0 (15)	61.2 (15)	81.0 (5)	46	50
3.2	3.436	247.0 (26)	64.2 (22)	80.8 (9)	53	41
4.8	3.479	260.2 (31)	67.7 (27)	81.0 (5)	42	44
5.3	3.492	271.0 (27)	68.1 (23)	80.5 (5)	52	39
5.9	3.507	278.0 (22)	70.3 (23)	81.1 (3)	37	58
7.3	3.542	292.3 (24)	72.9 (23)	80.9 (5)	38	41
7.6	3.549	294.2 (29)	73.1 (26)	80.7 (11)	54	35
8.4	3.569	300.0 (22)	75.4 (20)	80.6 (7)	42	47
9.7	3.599	310.9 (28)	77.8 (29)	80.4 (8)	40	47
9.8	3.602	313.1 (17)	78.4 (15)	80.2 (7)	60	56
11.1	3.631	323.7 (25)	80.8 (27)	79.9 (8)	54	54
17.3	3.762	383.0 (24)	88.5 (34)	78.8 (11)	89	39
17.9	3.775	386.0 (50)	90.1 (61)	79.0 (2)	34	55
18.8	3.793	400.7 (27)	95.0 (31)	78.8 (3)	79	40
23.0	3.871	437.6 (32)	102.2 (40)	77.5 (4)	80	40
25.2	3.910	470.5 (23)	105.9 (25)	76.5 (3)	72	33

[a]RMS, root-mean-square difference between observed and calculated sound velocities. Numbers in parentheses are 1 standard deviation uncertainty in the last digits.

tively inverted using Christoffel's equation. The inversion converged to a self-consistent density model and elastic constants (Table 2). Only the data collected up to 11.1 GPa were used to obtain the density model, because the alcohol mixture used as a pressure medium is known to become solid in the 11–12 GPa pressure range. The resulting elastic constants are shown in Figure 7.

[29] The Brillouin data obtained at pressures ranging from 17.3 to 25.2 GPa proved to be in excellent agreement with the extrapolation of the results from pressure below 11.1 GPa (Figure 7). The inversion also yielded the orientation of the sample platelet, which is (0 0.4 1). The overall precision (at 1σ level) of the moduli determination is 1% for C_{11} and C_{44} and 3% for C_{12}. The precision of the orientation determination is better than 2° on the Eulerian angle that relate the crystallographic reference system to the laboratory reference system [*Shimizu*, 1995]. No systematic variation of the recovered orientation was observed with pressure. The value of the moduli at room pressure and their pressure derivatives are reported in Table 3. The Hill average of the Voigt and Reuss bounds to the aggregate moduli are reported in Table 4.

[30] The longitudinal constant C_{11} and the off-diagonal constant C_{12} show a substantially linear increase through the whole experimental pressure range. C_{12} presents a slight curvature, which is detectable at the highest pressures (above 17.3 GPa) and is accurately described by the fit to a third-order Eulerian strain equation. The shear constant C_{44} reaches a maximum value of 81.1 GPa at 5.9 GPa. After 5.9 GPa its pressure derivative becomes negative. At a pressure of 25.2 GPa, C_{44} decreases to 76.5 GPa, and its pressure derivative reaches a value of −0.4.

[31] The elastic constants determined at standard conditions are in good agreement with the available data from ultrasonics techniques [*Son and Bartles*, 1972; *Chang and Graham*, 1977; *Oda et al.*, 1992], and they are within 10% of the athermal constants calculated by *Karki and Crain* [1998] using density functional theory (Table 3). The pressure derivatives of all the constants are lower than those determined by *Son and Bartles* [1972] based on measure-

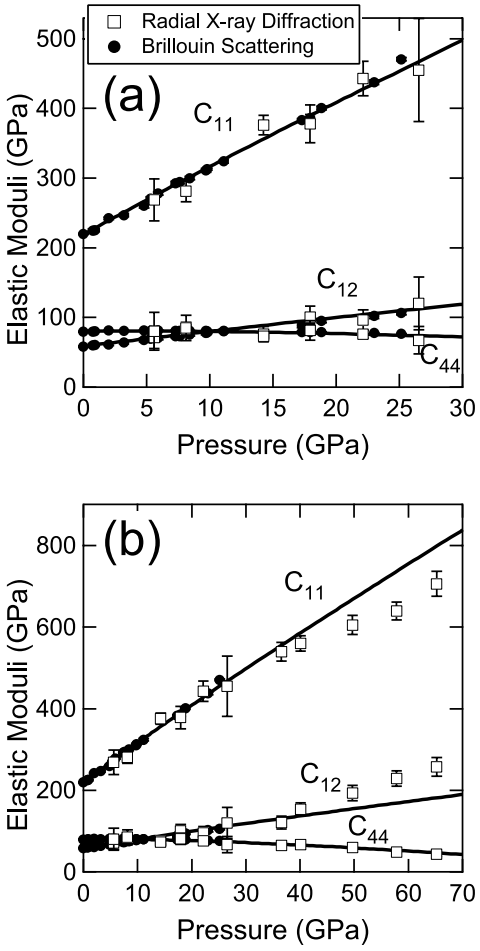

Figure 7. Individual elastic constants of CaO as a function of pressure. The lines are third-order Eulerian strain fits to the data. (a) Brillouin scattering experimental pressure range. (b) Complete radial X-ray diffraction experimental pressure range.

Table 3. Elastic Constants of CaO and Their Pressure Derivatives at Standard Conditions

Study[a]	C_{11}, GPa	C_{12}, GPa	C_{44}, GPa	$(\partial C_{11}/\partial P)_T$	$(\partial C_{12}/\partial P)_T$	$(\partial C_{44}/\partial P)_T$	P_{Max}, GPa
This study, Brillouin scattering	219.4 (7)	58.1 (7)	80.0 (2)	9.90 (1)	2.20 (1)	0.250 (3)	25
Ultrasonic interferometry							
S-B	223.0 (5)	59.0 (5)	81.0 (2)	10.30 (17)	3.90 (14)	0.600 (1)	0.2
C-G	221.9 (6)	57.8 (7)	80.3 (1)	10.36 (11)	2.09 (7)	0.196 (6)	1.0
Resonant ultrasound spectroscopy							
O	220.56 (4)	57.64 (3)	80.06 (1)				10^{-4}
Theory[b]							
K-C	239	51.6	77.4				

[a]Studies are S-B, *Son and Bartels* [1972]; C-G, *Chang and Graham* [1977]; O, *Oda et al.* [1992]; K-C, *Karki and Crain* [1998].
[b]Athermal parameters.

ments performed only up to 0.2 GPa. Our results for the pressure derivatives of C_{12} and C_{44} are comparable, within their respective uncertainties, with those of *Chang and Graham* [1977], who compressed CaO up to 1 GPa. However, the pressure derivative of C_{11} determined by Chang and Graham is more than 4% larger than the value determined in this study. If we consider that the pressure range explored in this study is more than 1 order of magnitude larger than that explored in previous studies, this discrepancy confirms analogous differences between the pressure derivatives of elastic moduli previously reported from the comparison of moderate- versus high-pressure studies, in other systems, both using X-ray diffraction and spectroscopic methods [e.g., *Zha et al.*, 1998].

[32] The Hill averages of the aggregate moduli determined in this study are in agreement with the results of previous elasticity measurements [*Son and Bartels*, 1972; *Chang and Graham*, 1977; *Oda et al.*, 1992] and with the results of the static compression study of *Richet et al.* [1988]. The pressure derivative of the shear modulus is in agreement with those of low-pressure ultrasonic studies, and that of the bulk modulus is in excellent agreement with the results of *Chang and Graham* [1977] but in large disagreement with those of *Soga* [1968] and *Son and Bartels* [1972]. The value of $(\partial K_T/\partial P)_{T0}$ that we obtain from Brillouin spectroscopy is more than 12% higher than the values determined from static compression by *Mammone et al.* [1981] and *Richet et al.* [1988]. However, this discrepancy does not preclude an overall consistency of the Brillouin isotherm with the experimental results of the X-ray diffraction studies due to the strong correlation between the bulk modulus and its pressure derivative in fitting volume-pressure data to an equation of state [e.g., *Angel*, 2000].

[33] The strong variation of the elastic anisotropy with pressure is one of the most interesting characteristics of CaO elastic behavior. The Zener anisotropy factor A, which is the square of the ratio of the acoustic velocity of the transverse mode propagating along [100] and that of the transverse mode propagating along [110] with $[1\bar{1}0]$ polarization, varies from 0.98 at 1 bar, which corresponds to an almost isotropic solid, to 0.42 at 25.2 GPa (Figure 3). Ab initio calculations show a systematic pressure induced decrease of the ratio between the longitudinal acoustic velocities along [110] and [100] in all the alkaline-earth oxides [*Tsuchiya and Kawamura*, 2001]. This effect can be explained using a spherical ionic model of these B1 structure oxides, because the higher compressibility of the oxygen ion causes a continuous increase of the cation/anion ratio and of the packing density along the [100] direction, with a consequent decrease of the ratio of the longitudinal velocities along [110] and [100]. The variation of anisotropy with pressure is dramatic in the case of MgO, which presents a reversal of

Table 4. Hill Average of the Reuss and Voigt Aggregate Bulk and Shear Moduli of CaO, and Their Pressure Derivatives at Standard Conditions

Study[a]	K_{S0}, GPa	K_{T0}, GPa	G_0, GPa	$(\partial K_S/\partial P)_{T0}$	$(\partial K_T/\partial P)_{T0}$	$(\partial G/\partial P)_{T0}$
This study, Brillouin scattering	112.00 (2)	110.7 (3)	80.05 (9)	4.72 (6)	4.80 (1)	1.69 (5)
Ultrasonic interferometry						
S[b]	105.90	104.9	76.1	5.23	5.26	
S-B	114.00 (3)		81.4 (6)	6.00 (1)		1.60
C-G	112.50 (59)	111.25	81.0 (1)	4.83 (7)	4.85	1.76
Resonant ultrasound spectroscopy						
O	111.95 (1)	110.60 (13)	80.62 (1)			
Theory[c]						
B	109		4.62			
M-C		122		4.52		
K-C		117	83.6	4.41		
X-ray diffraction						
M		115			4.1	
R		111 (1)			4.20 (2)	
Y		124			3.57	
Shock compression						
J-A	112			4.8		

[a]Studies are S, *Soga* [1968]; S-B, *Son and Bartels* [1972]; C-G, *Chang and Graham* [1977]; O, *Oda et al.* [1992]; B, *Bukowinski* [1985]; M-C, *Mehl et al.* [1988]; K-C, *Karki and Crain* [1998]; M, *Mammone et al.* [1981]; R, *Richet et al.* [1988]; Y, *Yamanaka et al.* [2002]; J-A, *Jeanloz and Ahrens* [1980].
[b]Polycrystalline sample.
[c]Athermal parameters.

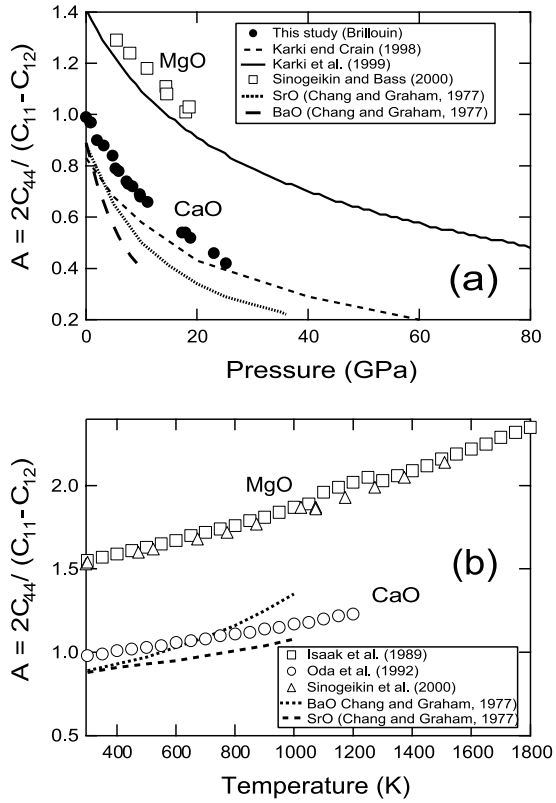

Figure 8. (a) Pressure dependence at ambient temperature of the elastic anisotropy expressed by Zener anisotropy factor $A = 2C_{44}/(C_{11} - C_{12})$ for CaO compared with other alkaline-earth oxides. (b) Temperature dependence at ambient pressure of Zener anisotropy factor, A, for CaO in comparison with other alkaline-earth oxides.

the anisotropy experimentally observed at about 20 GPa [*Duffy et al.*, 1995] and subsequently confirmed by theory [*Karki et al.*, 1997a] and by Brillouin experiments [*Sinogeikin and Bass*, 2000]. The effect is also observed in the oxides of heavier alkaline earth metals (Sr, Ba, and Ca) but the elastic anisotropy reversal occurs at high temperature (Figure 8). The elastic anisotropy factor A of CaO increases at high temperature and ambient pressure; it reaches the value of 1.23 at 1200 K [*Oda et al.*, 1992], consistent with the increase of A with increasing volume observed across all the alkaline earth oxides series.

[34] For MgO, the main process that generates the variation of the anisotropy ratio, A, is the stiffening of C_{11}. In the case of CaO, the stiffening of C_{11} is combined with softening of the shear constant C_{44} at pressures above 5.9 GPa. C_{44} softening in CaO precedes a structural phase transition to a high-pressure polymorph with CsCl-type structure, already well documented [e.g., *Jeanloz et al.*, 1979; *Mammone et al.*, 1981], that we also observed by X-ray diffraction at 57.8 GPa. The pressure at which we observed the transition is consistent both with previous static and dynamic compression experiments [*Jeanloz and Ahrens*, 1980; *Richet et al.*, 1988; *Yamanaka et al.*, 2002], and with first principles calculations [*Karki and Wentzkovitch*, 2003]. Softening of C_{44} is observed for both SrO and BaO [*Chang and Graham*, 1977] and confirmed by ab initio simulations [*Tsuchiya and Kawamura*, 2001] at lower pressure than for CaO, while for MgO it is not experimentally observed up to 55 GPa [*Zha et al.*, 2000] nor predicted theoretically at pressure below 300 GPa [*Karki et al.*, 1997b].

[35] At pressures between 8 and 11 GPa, the pressure derivative of C_{44} is already slightly negative. The Brillouin scattering data collected at pressure between 17.3 and 25.2 GPa confirm a slow decrease of C_{44} with pressure, in excellent agreement with the extrapolation of the fit to a third-order Eulerian equation [*Davies*, 1974]:

$$C_{ijkl} = (1+2f)^{7/2}\left[C^0_{ijkl} + a_1 f\right] - P\Delta_{ijkl}, \qquad (8)$$

where $f = 0.5[(V_0/V)^{2/3} - 1]$ is the Eulerian finite strain, C^0_{ijkl} is the value of the elastic constant at ambient conditions, $\Delta_{ijkl} = -\delta_{ij}\delta_{kl} - \delta_{ik}\delta_{jl} - \delta_{il}\delta_{jk}$ and P is the pressure. The coefficient a_1 is equal to $[3K_{T0}(\partial C^0_{ijkl}/\partial P + \Delta_{ijkl}) - 7C^0_{ijkl}]$, where K_{T0} and $\partial C^0_{ijkl}/\partial P$ are the isothermal bulk modulus and the pressure derivative of the elastic constant C_{ijkl} at ambient conditions.

[36] The vanishing of C_{44} at high pressure defines the mechanical instability of the NaCl structure for CaO, violating one of Born's stability criteria for solids with cubic symmetry [*Born and Huang*, 1954]. The extrapolated pressure at which C_{44} vanishes is 122 GPa, in disagreement with 177 GPa calculated at 0 K by *Karki et al.* [1997b] even taking into account the temperature effect. The reason of the apparent disagreement is caused by the systematic overestimation of volume by *Karki et al.* [1997b] [see also *Karki and Crain*, 1998]. The stability criterion, $C_{44} = 0$, is an upper bound to the transition pressure itself. The CsCl structure-type phase is predicted to become thermodynamically stable at pressure above 50 GPa [*Karki and Wentzkovitch*, 2003].

[37] The pressure dependence of C_{44} as determined from our Brillouin scattering data below $P = 11.1$ GPa can be adequately fitted with a third-order Eulerian strain equation. It can also be fitted to a fourth-order Eulerian strain equation of the form [*Davies*, 1974]

$$C_{ijkl} = (1+2f)^{7/2}\left[C^0_{ijkl} + a_1 f + 0.5 a_2 f^2\right] - P\Delta_{ijkl}, \qquad (9)$$

where $a_2 = 9K^2_{T0}\partial^2 C^0_{ijkl}/\partial P^2 + 3\partial K_{T0}/\partial P(a_1 + 7C^0_{ijkl}) - 16a_1$ $16a_1 - 49C^0_{ijkl}$, and $\partial^2 C^0_{ijkl}/\partial P^2$ and $\partial K_{T0}/\partial P$ are the second pressure derivative of the elastic constant and the first pressure derivative of the isothermal bulk modulus at ambient conditions, respectively. Equation (9) represents the next order expansion of (8) in Eulerian strain.

[38] The quality of the fit to the third-order and to the fourth-order equations is not significantly distinguishable. The parameters of the fourth-order fitting are $C_{44} = 79.5$ (2) GPa, $\partial C_{44}/\partial P = 0.6$ (1), $\partial^2 C_{44}/\partial P^2 = -0.12$ (3) GPa^{-1}. The "fourth-order" extrapolated C_{44} vanishes at 59 GPa. Because of the strong curvature of the fourth-order equation the extrapolated values of C_{44} differ as much as 14% from the data that we collected at 25.2 GPa. We decided to reject the fourth-order fit because the limited experimental pressure range does not guarantee sufficient constraint on the second-order pressure derivative of C_{44}.

Table 5. Experimental Compression and Best Fit Elastic Constants of CaO From Radial X-Ray Diffraction

Pressure, GPa	V/V_0	C_{11}, GPa	C_{12}, GPa	C_{44}, GPa	A^a (X-Ray)	t, GPa	α^b	A (Brillouin)	t_{111}, GPa	t_{200}, GPa	t_{220}, GPa
5.6	0.9471	270 (30)	70 (16)	81 (27)	0.80 (2)	0.3 (1)	0.90 (3)	0.79 (2)	0.24 (9)	0.27 (6)	0.40 (1)
8.1	0.9236	281 (11)	81 (8)	85 (17)	0.90 (1)	0.4 (2)	0.5 (3)	0.72 (1)	0.43 (3)	0.38 (1)	0.25 (4)
14.3	0.9064	384 (36)	75 (19)	75 (13)	0.49 (1)	0.9 (1)	1.0 (–)	0.49 (1)	0.83 (7)	0.85 (4)	0.86 (3)
17.9	0.8794	378 (33)	102 (19)	80 (17)	0.58 (8)	1.0 (1)	0.80 (2)	0.52 (8)	1.40 (1)	0.90 (2)	0.55 (8)
22.1	0.8659	440 (70)	99 (36)	75 (22)	0.44 (3)	1.1 (3)	1.00 (1)	0.46 (3)	1.14 (5)	1.13 (9)	1.00 (1)
26.5	0.8451	477 (105)	109 (53)	73 (29)	0.40 (6)	0.9 (4)	1.00 (1)	0.41 (6)	1.00 (5)	1.00 (1)	0.84 (5)
36.6	0.8139	561 (46)	131 (26)	68 (10)	0.32 (1)	1.4 (2)	0.99 (3)	0.31 (1)	1.41 (4)	1.42 (7)	1.50 (1)
40.1	0.7988	561 (42)	153 (23)	67 (11)	0.33 (2)	1.6 (2)	0.88 (5)	0.28 (2)	1.50 (1)	1.56 (7)	1.80 (2)
49.7	0.7794	605 (49)	185 (28)	61 (10)	0.29 (2)	1.1 (2)	0.83 (3)	0.23 (2)	0.90 (6)	1.35 (5)	1.00 (1)
57.8	0.7562	679 (65)	223 (36)	54 (11)	0.24 (1)	1.8 (4)	0.82 (4)	0.18 (1)	1.81 (8)	2.40 (2)	1.70 (2)
65.2	0.7344	716 (183)	244 (100)	48 (26)	0.20 (2)	1.1 (3)	0.82 (8)	0.15 (2)	1.20 (1)	1.00 (5)	0.90 (3)

[a] A, $2C_{44}/(C_{11} - C_{12})$.
[b] Values determined by fixing A to the values from Brillouin scattering.

4.2. Radial Diffraction

[39] The radial X-ray diffraction data were analyzed following the model outlined by *Singh et al.* [1998a] assuming stress continuity across grain boundaries ($\alpha = 1$, see section 3.2). The results of the inversion are reported in Table 5. The hydrostatic pressures and the cell parameter for CaO at each pressure (see section 3.2 for details on the data analysis), were fitted to a third-order Birch-Murnaghan equation of state fixing the unit cell parameter at ambient conditions to our experimental value. The inversion yielded a bulk modulus K_{T0} = 110 (5) GPa and its pressure derivative $(\partial K_T/\partial P)_{T0}$ = 4.5 (4). Fixing K_{T0} = 110.7 GPa from the Brillouin results gives $(\partial K_T/\partial P)_{T0}$ equal to 4.4 (5), in agreement with our Brillouin results. The agreement between the 300 K isotherm from radial X-ray diffraction and from Brillouin scattering is excellent along the whole common pressure range, and it extends, within reciprocal uncertainties up to 36.6 GPa.

[40] The extrapolation above 36.6 GPa produces inconsistency between the Brillouin isotherm and the X-ray diffraction data (Figure 9). The discrepancy can be reconciled introducing a higher-order term in the Eulerian strain equation for the bulk modulus. The new fit parameter, $(\partial^2 K_T/\partial P^2)_{T0} = -0.08$ (6) GPa^{-1}, does not visibly improve the quality of the fitting of the Brillouin data obtained with the third-order Eulerian equation (which, because of truncation, constrains $(\partial^2 K_T/\partial P^2)_{T0}$ to an effective value of -0.05 GPa^{-1}). The fourth-order isotherm is in excellent agreement with the X-ray diffraction data (Figure 9) at high pressure suggesting that a possible softening of the pressure derivative of the bulk modulus is present at pressures ranging between 40 and 60 GPa. The apparent softening might be related to the phase transition to a CsCl structured polymorph that we observed at 57.8 GPa.

[41] Even though our X-ray diffraction data are in reasonable agreement with previous results [*Mammone et al.*, 1981; *Richet et al.*, 1988; *Yamanaka et al.*, 2002], it is interesting to notice the large disagreement between the equation of state parameters determined in the different studies (Table 4). The discrepancies in the fitted parameters are not entirely justified by the experimental results (Figure 9) but are caused by the strong correlation between the bulk modulus and its pressure derivatives discussed earlier. Placing constraints on the value of the bulk modulus by direct elasticity measurements solves this problem.

[42] By fitting the values of $Q(hkl)$ and $\Gamma(hkl)$ for all the diffraction lines with a linear relation we could determine Zener anisotropy factor, A (Table 5). The retrieved elastic anisotropy increases in magnitude (i.e., Zener anisotropy factor decreases below 1) with pressure, in good agreement with the experimental Brillouin data and their extrapolation (Figure 10). The differential stress, t, determined using

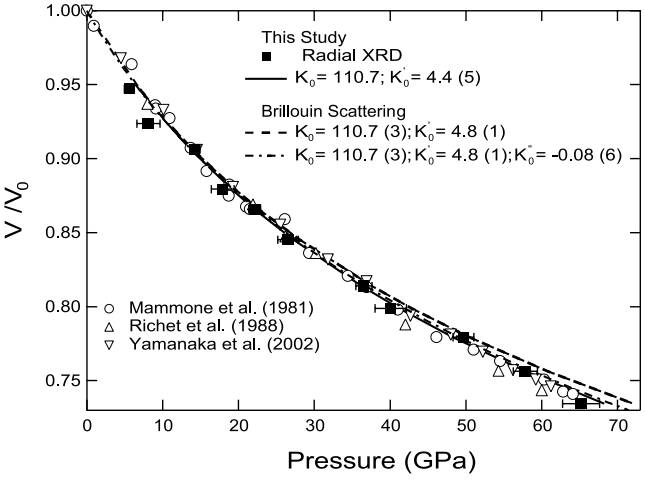

Figure 9. The 300 K isotherm of CaO determined by inversion of the hydrostatic compression measured by radial diffraction to the third-order Birch-Murnaghan equation of state. Existing static compression data are plotted for comparison. $K_0' = (\partial K_T/\partial P)_{T0}$; $K_0'' = (\partial^2 K_T/\partial P^2)_{T0}$.

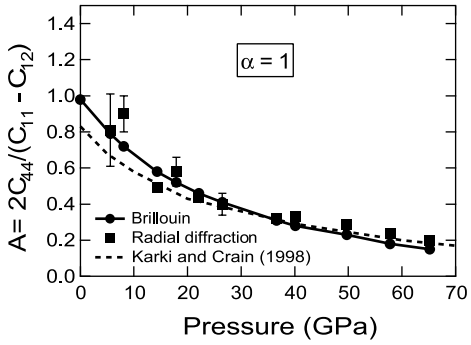

Figure 10. Elastic anisotropy of CaO, expressed by the Zener factor, A (see section 3.2), as a function of pressure. Brillouin results and radial X-ray diffraction estimations are plotted together for comparison.

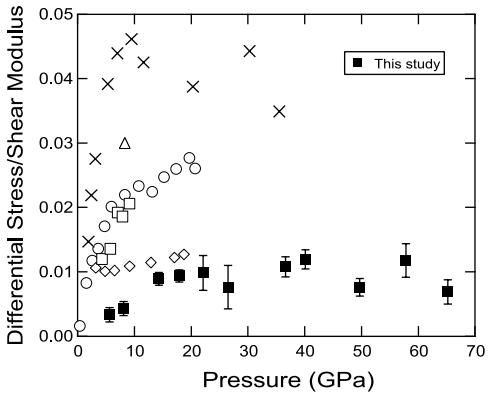

Figure 11. Normalized uniaxial stress component in CaO compressed under nonhydrostatic conditions. The results of this study are compared with the high-pressure strength of other isostructural binary compounds. Solid squares, this study; open diamonds, NaCl from *Funamori et al.* [1994]; open circles, MgO from *Uchida et al.* [1996]; open triangles, FeO from *Singh et al.* [1998b]; open squares, FeO from *Dubrovinsky et al.* [2000]; crosses, MgO from *Merkel et al.* [2002].

equation (7) increases from 0.3 to 1.9 GPa, in the range between 5.6 and 57.8 GPa (Table 5). A decreased value, 1.1 GPa, calculated at the maximum experimental pressure, might be related to the presence of coexisting NaCl-type and CsCl-type polymorphs, as detected by X-ray diffraction.

[43] The ratio of differential stress to shear modulus, t/G, is plotted in Figure 11 in comparison with other compounds with NaCl-type structure. It is evident from Figure 11, that MgO and FeO present a relatively larger strength than CaO and NaCl, which are characterized by more ionic bonding. Vanishing of the pressure dependence of t/G above 17.9 GPa could also be interpreted as an indication of large plastic flow or a change in the deformation mechanism.

[44] The Zener anisotropy factor from radial diffraction, together with the extrapolated shear modulus and bulk modulus, were used to also estimate the elastic constants at high pressure using the procedure outlined by *Singh et al.* [1998a]. Because of the observed consistency between the aggregate bulk modulus determined by Brillouin and X-ray diffraction, we constrained it to the values from Brillouin at the relevant pressures, after conversion to isothermal conditions. The estimated elastic constants are reported in Table 5.

[45] At $P < 36.6$ GPa the calculated X-ray elastic constants are in good agreement with those determined by Brillouin spectroscopy and their extrapolation (Figure 7). At pressure higher than 36.6 GPa we observed an increasing discrepancy of the value of C_{11} and C_{12} with respect to the extrapolation from Brillouin data. C_{11} is 12% softer and C_{12} is 40% stiffer than the extrapolation of Brillouin data at the maximum pressure of 65.2 GPa.

[46] In the lattice strain equations a strong correlation exists between the value of t, and the parameter α, which defines the boundary conditions in the analysis of the elastic response of the sample. In order to evaluate the value of the parameter α, we fixed the elastic constants using our Brillouin results and determining α from equation (5). The results are shown in Table 5. The value of α is constrained to 1.0 (2) at pressure between 14.3 GPa and 36.6 GPa. Then it decreases and it reaches a constant value of 0.82 (8) at pressures above 49.7 GPa (Figure 12). The interpretation of the data at pressure below 14.3 GPa is unclear. It is possible that the sample is still undergoing changes in the geometric relationship between grains due to incomplete compaction.

[47] Recent independent results for MgO at pressures in the range between 2 and 6 GPa at 500°C [*Weidner et al.*, 2004] and in the pressure range between 0 and 8 GPa at ambient temperature [*Uchida et al.*, 2004] have demonstrated that the onset of plastic deformation substantially changes the behavior of powder materials in uniaxial compression devices potentially causing large violations of the assumptions of lattice strain theory. The discrepancy between the extrapolated elastic constants from Brillouin measurements and the calculated elastic constants from radial X-ray diffraction data could also be affected by plastic deformation of the sample, which results in large heterogeneity of the uniaxial stress supported by subpopulations of crystallites with different orientation, as also suggested by *Singh* [2000]. The existence of this effect would cause large deviations from the linear dependence of the measured d spacings with respect to the orientation parameter, $1-3\cos^2\psi$ (see section 3.2), that we did not observe within our experimental resolution.

[48] Fixing the value of the elastic constants to the results of Brillouin measurement, we can also invert the radial diffraction data to estimate the microscopic yield stress, $t(hkl)$, defined as [*Singh et al.*, 1998a]

$$Q(hkl) = t(hkl)/3[S_{11} - S_{12} - 3\Gamma(hkl)(S_{11} - S_{12} - S_{44}/2)] \quad (10)$$

along slip directions in the relevant slip planes. Following *Singh* [2000], in the plastic deformation regime, the value of $t(hkl)$ is directly related to the orientation average of the critical resolved shear stress for the selected slip system. In the case of competing slip systems, the one with the lowest critical stress, i.e., the lowest $t(hkl)$, is operative and progressive texturing could cause systematic differences

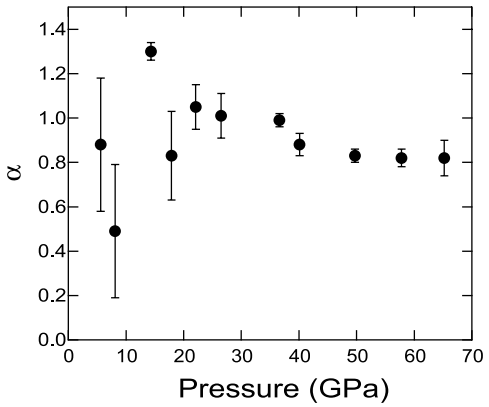

Figure 12. Variation of the parameter α for CaO with pressure. The value of α was calculated using equation (5) (see text for details).

between $t(hkl)$ for the different lattice planes. The values of $t(200)$, $t(220)$, $t(111)$, which are all potential slip planes in the B1 structure, were calculated using the elastic constants determined by Brillouin scattering and the $Q(hkl)$ determined from radial X-ray diffraction. However, the present results (Table 5) show that $t(200)$, $t(220)$, and $t(111)$ fluctuate at each pressure about their overall average value, without any systematic pressure effect and so no clear evidence for plastic anisotropy can be identified.

5. Conclusions

[49] The combination of Brillouin scattering measurements and radial X-ray diffraction allowed us to better constrain the elasticity of CaO at high pressure. Over the common pressure range, the results of the two sets of measurements are in agreement within a few percent. The parameters of the 300 K isotherm from Brillouin scattering, are, K_{T0} = 110.7 (3), $(\partial K_T/\partial P)_{T0}$ = 4.8 (1). The results of X-ray diffraction to 65.2 GPa suggest a softening of the equation of state probably related to the approaching transition to a high-pressure polymorph. Brillouin scattering in the pressure range between 17.3 and 25.2 GPa shows softening of C_{44}. The extrapolated pressure at which the crystal structure is mechanically unstable is 122 GPa. Radial X-ray diffraction allow us to determine the high-pressure strength of CaO, which increases from 0.3 to 1.9 GPa in the pressure range between 5.6 and 57.8 GPa, and to determine the elastic anisotropy and the elastic constants. Over the common experimental range and upon extrapolation to 36.6 GPa, the two methods are in excellent agreement. At pressure above 36.6 GPa, C_{11} becomes as much as 12% softer and C_{12} as much as 40% stiffer than the extrapolation of Brillouin data. The discrepancy between Brillouin extrapolations and radial diffraction results can be reconciled by a decrease of α, the parameter describing stress/strain continuity across grain boundaries in the sample, from 1 at 36.6 GPa to 0.82 at 65.2 GPa. However, the possible effects of plastic deformation cannot be ruled out at present.

[50] **Acknowledgments.** We thank J. Hu of X17C at NSLS for experimental assistance. We thank S.-H. Shim for providing Figure 1. We also thank F. Jiang, B. Kiefer, and S. Hongsresawat for comments and helpful discussion. We thank the Editor and two anonymous reviewers for their thoughtful comments. This work was supported by the NSF and the David and Lucile Packard Foundation. Portions of this research were carried out at the National Synchrotron Light Source, Brookhaven National Laboratory, which is supported by the U.S. Department of Energy. S.S. acknowledges support by the Miller Institute for Basic Research in Science.

References

Angel, R. J. (2000), Equations of state, in *High-Temperature and High-Pressure Crystal Chemistry*, *Rev. Mineral. Geochem.*, vol. 41, edited by R. M. Hazen and R. T. Downs, pp. 35–59, Mineral. Soc. of Am., Washington, D. C.

Antonangeli, D., F. Occelli, H. Requardt, J. Badro, G. Fiquet, and M. Krisch (2004), Elastic anisotropy in textured hcp-iron to 112 GPa from sound wave propagation measurements, *Earth Planet. Sci. Lett.*, *225*, 243–251.

Auld, B. (1973), *Acoustic Fields and Waves in Solids*, vol. 1, John Wiley, Hoboken, N. J.

Barsch, G. R. (1967), Adiabatic, isothermal, and intermediate pressure derivatives of the elastic constants for cubic symmetry, *Phys. Stat. Solids*, *19*, 129–138.

Born, M., and K. Huang (1954), *Dynamical Theory of Crystal Lattices*, Oxford Univ. Press, New York.

Bukowinski, M. S. T. (1985), First principles equations of state of MgO and CaO, *Geophys. Res. Lett.*, *12*, 536–539.

Chang, Z. P., and E. K. Graham (1977), Elastic properties of oxides in the NaCl structure, *J. Phys. Chem. Solids*, *38*, 1355–1362.

Davies, G. F. (1974), Effective elastic moduli under hydrostatic stress, I, Quasi-harmonic theory, *J. Phys. Chem. Solids*, *35*, 1513–1520.

Davies, G. F., and A. M. Dziewonski (1975), Homogeneity and constitution of the Earth's lower mantle and outer core, *Phys. Earth Planet. Inter.*, *10*, 336–343.

Dubrovinsky, L., N. Dubrovinskaia, S. Saxena, and T. LiBehan (2000), X-ray diffraction under non-hydrostatic conditions in experiments with diamond anvil cell: Wüstite (FeO) as an example, *Mater. Sci. Eng. A*, *288*, 187–190.

Duffy, T. S., and D. L. Anderson (1989), Seismic velocities in mantle minerals and the mineralogy of the upper mantle, *J. Geophys. Res.*, *94*, 1895–1912.

Duffy, T. S., R. J. Hemley, and H.-K. Mao (1995), Equation of state and strength at multimegabar pressure: Magnesium oxide to 227 GPa, *Phys. Rev. Lett.*, *74*, 1371–1374.

Duffy, T. S., G. Shen, D. L. Heinz, J. Shu, Y. Ma, H.-K. Mao, R. J. Hemley, and A. K. Singh (1999a), Lattice strains in gold and rhenium under nonhydrostatic compression to 37 GPa, *Phys. Rev. B.*, *60*, 15,063–15,073.

Duffy, T. S., G. Shen, J. Shu, H.-K. Mao, R. J. Hemley, and A. K. Singh (1999b), Elasticity, shear strength, and equation of state of molybdenum and gold from X-ray diffraction under nonhydrostatic compression to 24 GPa, *J. Appl. Phys.*, *86*, 6729–6736.

Funamori, N., T. Yagi, and T. Uchida (1994), Deviatoric stress measurements under uniaxial compression by powder X-ray diffraction method, *J. Appl. Phys.*, *75*, 4327–4331.

Garvin, D., V. B. Parker, and H. J. White (Eds.) (1987), *Codata Thermodynamic Tables: Selections for Some Compounds of Calcium and Related Mixtures: A Prototype Set of Tables*, 356 pp. Taylor and Francis, Philadelphia, Pa.

Isaak, D. G., O. L. Anderson, and T. Goto (1989), Measured elastic modulus of single-crystal MgO up to 1800 K, *Phys. Chem. Miner.*, *16*, 704–713.

Jeanloz, R., and T. J. Ahrens (1980), Equation of state of FeO and CaO, *Geophys. J. R. Astron. Soc.*, *62*, 505–528.

Jeanloz, R., T. J. Ahrens, H.-K. Mao, and P. M. Bell (1979), B1-B2 transition in calcium oxide from shock-wave and diamond-cell experiments, *Science*, *206*, 829–830.

Karato, S. I., and B. B. Karki (2001), Origin of lateral variation of seismic waves velocities and density in the deep mantle, *J. Geophys Res.*, *106*, 21,771–21,783.

Karato, S. I., and P. Wu (1993), Rheology of the upper mantle: A synthesis, *Science*, *260*, 771–778.

Karki, B. B., and J. Crain (1998), Structure and elasticity of CaO at high pressure, *J. Geophys. Res.*, *103*, 12,405–12,411.

Karki, B. B., and R. M. Wentzkovitch (2003), Vibrational and quasiharmonic thermal properties of CaO under pressure, *Phys. Rev. B*, *68*, 22434, doi:11.03/PhysRevB.68.224304.

Karki, B. B., L. Stixrude, S. J. Clark, M. C. Warren, G. J. Ackland, and J. Crain (1997a), Structure and elasticity of MgO at high pressure, *Am. Mineral.*, *82*, 51–60.

Karki, B. B., G. J. Ackland, and J. Crain (1997b), Elastic instabilities in crystals from ab initio stress-strain relations, *J. Phys. Condens. Matter*, *9*, 8579–8589.

Karki, B. B., R.M. Wentzkovitch, S. de Gironcoli, and S. Baroni (1999), Elastic anisotropy and wave velocities of MgO at lower mantle conditions, *Science*, *286*, 1705–1707.

Liebermann, R. C., and B. Li (1998), Elasticity at high-pressures and temperatures, in *Ultrahigh-Pressure Mineralogy: Physics and Chemistry of the Earth*'s *Deep Interior*, *Rev. Mineral.*, vol. 37, edited by R. J. Hemley, pp. 459–492, Mineral. Soc. of Am., Washington, D. C.

Mammone, J. F., H.-K. Mao, and P. M. Bell (1981), Equation of state of CaO under static pressure conditions, *Geophys. Res. Lett.*, *8*, 140–142.

Mao, H.-K., J. Xu, and P. M. Bell (1986), Calibration of the ruby pressure gauge to 800 kbar under quasi-hydrostatic conditions, *J. Geophys. Res.*, *91*, 4673–4677.

Mao, H.-K., J. Shu, G. Shen, R. J. Hemley, B. Li, and A. K. Singh (1998), Elasticity and rheology of iron above 220 GPa and the nature of the Earth's inner core, *Nature*, *396*, 741–743, Correction, 1999. *Nature. 399*, 280.

Matthies, S., S. Merkel, H. R. Wenk, R. J. Hemley, and H.-K. Mao (2001), Effects of texture on the determination of elasticity of polycrystalline ε-iron from diffraction measurements, *Earth Planet. Sci. Lett.*, *194*, 201–212.

Meade, C., and R. Jeanloz (1988), Yield strength of MgO to 40 GPa, *J. Geophys. Res.*, *93*, 3261–3269.

Mehl, M. J., R. E. Cohen, and H. Krakauer (1988), Linearized augmented plane wave electronic structure calculation for MgO and CaO, *J. Geophys. Res.*, *93*, 8009–8022.

Merkel, S., A. F. Goncharov, H. K. Mao, P. Gillet, and R. J. Hemley (2000), Raman spectroscopy of iron to 152 gigapascals: Implications for Earth's inner core, *Science*, *288*, 1626–1629.

Merkel, S., H. R. Wenk, J. Shu, G. Shen, P. Gillet, H. Mao, and R. J. Hemley (2002), Deformation of polycrystalline MgO at pressures of the lower mantle, *J. Geophys. Res.*, *107*(B11), 2271, doi:10.1029/2001JB000920.

Merrill, L., and W. A. Bassett (1974), Miniature diamond-anvil pressure cell for single-crystal X-ray diffraction, *Rev. Sci. Instrum.*, *45*, 290–294.

Oda, H., O. L. Anderson, D. G. Isaak, and I. Suzuki (1992), Measurement of elastic properties of single-crystal CaO up to 1200K, *Phys. Chem. Miner.*, *19*, 96–105.

Oliver, W. F., C. A. Herbst, S. M. Lindsay, and G. H. Wolf (1992), A general method for determination of Brillouin linewidths by correction for instrumental effects and aperture broadening: Application to high-pressure diamond anvil cell experiments, *Rev. Sci. Instrum.*, *63*, 1884–1895.

Richet, P., H.-K. Mao, and P. M. Bell (1988), Static compression and equation of state of CaO to 1.35 Mbar, *J. Geophys. Res.*, *93*, 15,279–15,288.

Ruoff, A. L. (1975), Stress anisotropy in opposed anvil high-pressure cells, *J. Appl. Phys.*, *46*, 1389–1392.

Shimizu, H. (1995), High-pressure Brillouin scattering of molecular single-crystals grown in a diamond-anvil cell, in *High Pressure Research on Solids*, edited by M. Senoo et al., pp. 1–17, Elsevier, New York.

Singh, A. K. (1993), The lattice strains in a specimen (cubic system) compressed nonhydrostatically in an opposed anvil device, *J. Appl. Phys.*, *73*, 4278–4286.

Singh, A. K. (2000), Lattice strains under non-hydrostatic compression, in *Science and Technology of High Pressure*, *Proceedings of XVII AIRAPT*, edited by M. H. Manghnani, W. J. Nellis, and M. F. Nicol, pp. 62–67, Univ. Press, Hyderabad, India.

Singh, A. K., and G. C. Kennedy (1974), Uniaxial stress component in tungsten carbide anvil high-pressure cameras, *J. Appl. Phys.*, *45*, 4686–4691.

Singh, A. K., C. Balasingh, H.-K. Mao, R. J. Hemley, and J. Shu (1998a), Analysis of lattice strains measured under nonhydrostatic pressure, *J. Appl. Phys.*, *83*, 7567–7575.

Singh, A. K., H.-K. Mao, J. Shu, and R. J. Hemley (1998b), Estimation of single-crystal elastic moduli from polycrystalline X-ray diffraction at high pressure: Application to FeO and iron, *Phys. Rev. Lett.*, *80*, 2157–2160.

Sinogeikin, S. V., and J. D. Bass (2000), Single-crystal elasticity of pyrope and Mgo to 20 GPa by Brillouin scattering in the diamond anvil cell, *Phys. Earth Planet. Inter.*, *120*, 43–62.

Sinogeikin, S. V., J. M. Jackson, B. O'Neill, J. W. Palko, and J. D. Bass (2000), Compact high-temperature cell for Brillouin scattering measurements, *Rev. Sci. Instrum.*, *71*, 1–6.

Soga, N. (1968), Elastic properties of CaO under pressure and temperature, *J. Geophys. Res.*, *73*, 5385–5390.

Son, P. R., and R. A. Bartels (1972), CaO and SrO single crystal elastic constants and their pressure derivatives, *J. Phys. Chem. Solids*, *33*, 828–829.

Speziale, S., and T. S. Duffy (2002), Single-crystal elasticity of fluorite (CaF_2) to 9.3 GPa, *Phys. Chem. Miner.*, *29*, 465–472.

Steinle-Neumann, G., L. Stixrude, and R. E. Cohen (1999), First-principles elastic constants for the hcp transition metals Fe, Co, and Re at high pressure, *Phys. Rev. B*, *60*, 791–799.

Tsuchiya, T., and K. Kawamura (2001), Systematics of elasticity: Ab initio study in B1-type alkaline earth oxides, *J. Chem. Phys.*, *114*, 10,086–10,093.

Uchida, T., N. Funamori, T. Ohtani, and T. Yagi (1996), Differential stress of MgO and Mg_2SiO_4 under uniaxial stress field: Variation with pressure, temperature, and phase transition, in *High Pressure Science and Technology, Proceedings of Joint XV AIRAPT and XXXIII EHPRG International Conference*, edited by W. A. Trzeciakowski, pp. 183–185, World Sci., Hackensack, N. J.

Uchida, T., Y. Wang, M. L. Rivers, and S. R. Sutton (2004), Yield strength and strain hardening of MgO up to 8 GPa measured in the deformation-DIA with monochromatic X-ray diffraction, *Earth Planet. Sci. Lett.*, *226*, 117–126.

Weidner, D. J., L. Li, M. Davis, and J. Chen (2004), Effect of plasticity on elastic modulus measurements, *Geophys. Res. Lett.*, *31*, L06621, doi:10.1029/2003GL019090.

Wenk, H. R., I. Lonardelli, J. Pehl, J. Devine, V. Prakapenka, G. Shen, and H. K. Mao (2004), In situ observation of texture development in olivine, ringwoodite, magnesiowüstite and silicate perovskiteat high pressure, *Earth Planet. Sci. Lett.*, *226*, 507–519.

Withfield, C. H., E. M. Brody, and W. A. Bassett (1976), Elastic moduli of NaCl by Brillouin scattering at high pressure in a diamond anvil cell, *Rev. Sci. Instrum.*, *47*, 942–947.

Wyckoff, R. W. G. (1963), *Crystal Structures*, John Wiley, Hoboken, N. J.

Yamanaka, T., K. Kittaka, and T. Nagai (2002), B1-B2 transition in CaO and possibility of $CaSiO_3$-perovskite decomposition under high pressure, *J. Mineral. Petrol. Sci.*, *97*, 144–152.

Zha, C.-S., T. S. Duffy, R. T. downs, H.-K. Mao, and R. J. Hemley (1998), Brillouin scattering and X-ray diffraction of San Carlos olivine: Direct pressure determination to 32 GPa, *Earth Planet. Sci. Lett.*, *159*, 25–33.

Zha, C.-S., H.-K. Mao, and R. J. Hemley (2000), Elasticity of MgO and a primary pressure scale to 55 GPa, *Proc. Natl. Acad. Sci. U.S.A.*, *97*, 13,494–13,499.

Zhao, Y., A. C. Lawson, J. Zhang, B. I. Bennett, and R. B. Von Dreele (2001), Thermoelastic equation of state of molybdenum, *Phys. Rev. B*, *62*, 8766–8776.

T. S. Duffy, Department of Geosciences, Princeton University, Princeton, NJ 08544, USA.

S. R. Shieh, Department of Earth Sciences, University of Western Ontario, London, Ontario, Canada N6A 5B7.

S. Speziale, Department of Earth and Planetary Science, University of California, Berkeley, CA 94720, USA. (speziale@uclink.berkeley.edu)